Journal of Environmental Management 264 (2020) 110477

Contents lists available at ScienceDirect

Journal of Environmental Management

journal homepage: http://www.elsevier.com/locate/jenvman

Research article

Use of nano-/micro-magnetite for abatement of cadmium and lead contamination

Zeeshan Ajmal [a,b], Muhammad Usman [a,c,*], Ioannis Anastopoulos [d], Abdul Qadeer [a,e], Runliang Zhu [f], Abdul Wakeel [a], Renjie Dong [b]

[a] Institute of Soil and Environmental Sciences, University of Agriculture, Faisalabad, 38040, Pakistan
[b] MoA Key Laboratory for Clean Production and Utilization of Renewable Energy, MoST National Center for International Research of BioEnergy Science and Technology, College of Engineering, China Agricultural University, 100083, Beijing, China
[c] PEIE Research Chair of Public Establishment for Industrial Estates and Free Zones, Center for Environmental Studies and Research, Sultan Qaboos University, Al-Khoud 123, Muscat, Oman
[d] Radioanalytical and Environmental Chemistry Group, Department of Chemistry, University of Cyprus, P.O. Box 20537, Nicosia, CY-1678, Cyprus
[e] Key Laboratory of Geographic Information Science of the Ministry of Education, School of Geographical Sciences, East China Normal University, Shanghai, 200241, China
[f] Guangzhou Institutes of Geochemistry, Chinese Academy of Sciences, 510640, Guangzhou, China

ARTICLE INFO

Keywords:
Metal contamination
Magnetite
Nanotechnology
Adsorption
Metal immobilization
Soil remediation

ABSTRACT

Structural variations of a mineral dictate its adsorption capacity which affects the mobility and toxicity of contaminants in natural and engineered systems. Present batch study evaluates the adsorption of lead (Pb) and cadmium (Cd) onto three magnetites having nanometric (M1-30 nm and M2-60 nm) and micrometric particle sizes (M3-1.5 μm). Obtained data revealed that particle size of tested magnetites strongly affected the extent and kinetics of metal adsorption and desorption. Observed order of adsorption efficiency was M1 > M2 > M3 with optimum monolayer adsorption of 408.14, 331.40, 178.47 mg/g (for Pb) and 228.05, 170.86, 83.49 mg/g (for Cd), respectively. Adsorption data were well fitted to the Freundlich (R^2 = 0.99), Langmuir (R^2 = 0.99) and pseudo-first order models (R^2 = 0.98). Electrostatic attraction and surface precipitation interaction via external mass transfer between bulk liquid-solid interfaces were the potential adsorption pathways. Pb showed higher affinity than Cd in multi-metal system. Desorption efficiency was higher in acidic environment (92%) than in distilled water (44%). Moreover, regenerated magnetite samples retained good adsorption capacity for six cycles. As soils are characterized by large variability of iron minerals, these findings have important implications regarding the transport and immobilization of contaminants particularly in the management of contaminated soils.

1. Introduction

Presence of toxic metals in the aquatic and soil environment poses serious threats to the environment and public health (Hamid et al., 2019a, b). Situation is worsening in developing countries like Pakistan, where industries are disposing metal-contaminated wastewater into local water bodies without proper treatment (Murtaza et al., 2017). Contaminated wastewater is being used for agricultural purposes due to the prevailing water shortage which leads to the entry of metals into the agricultural soils and ultimately the food chain (Hamid et al., 2019c). Considering the non-biodegradable nature of metals, strong persistence in soils, and their higher tendency to bioaccumulate in living organisms (Fu and Wang, 2011), finding suitable strategies to address metal contamination has received significant attention among the scientific community.

There exist different remediation strategies with varying treatment efficiency. Adsorption is usually considered as an effective technique which can bind the pollutants in a quick and cost-effective way that reduces their bioavailability and toxicity (Hamid et al., 2020). Iron minerals are abundant in environment and are widely used for soil immobilization and wastewater treatment (Hamid et al., 2019a). Magnetite, a mixed-valent Fe oxide denoted as [$Fe(II)Fe(III)_2O_4$], is a

* Corresponding author. PEIE Research Chair for the Development of Industrial Estates and Free Zones, Center for Environmental Studies and Research, Sultan Qaboos University, Al-Khoud 123, Muscat, Oman.
E-mail address: muhammad.usman@squ.edu.om (M. Usman).

https://doi.org/10.1016/j.jenvman.2020.110477
Received 26 December 2019; Received in revised form 27 February 2020; Accepted 22 March 2020
Available online 31 March 2020

ubiquitous iron oxide in soils and sediments formed by different abiotic and biotic pathways (Cornell and Schwertmann, 2003). Magnetite plays a prominent role in dictating the mobility and toxicity of various pollutants and in biogeochemical cycling of trace elements in soil. It is amongst the highly efficient adsorbent due to its high adsorption capacity, stability and magnetic nature (Usman et al., 2018). Its ferromagnetic nature facilitates its separation from the reaction medium for pollutant recovery and repeated adsorption (Ajmal et al., 2020; Fu et al., 2019). It should be noted that formation pathways control the structural properties and composition of magnetite and, therefore, large variability of magnetite is found in natural soils and sediments (Usman et al., 2018).

Adsorptive interaction of magnetite has been reported with different metal ions such as As (Yean et al., 2005), Cd, Cu, Ni and Pb (Nassar, 2010), Cr (Parsons et al., 2014), U etc. (Singer et al., 2012). However, limited information is available regarding adsorption of metal ions onto different magnetites that merits to be studied considering the existence of large variability of magnetite as micrometric and nanometric particles in natural and engineered settings. Adsorption efficiency is mainly dictated by characteristics of reaction medium and that of adsorbent. Structural variations and heterogeneity of a mineral could dictate its pollutant adsorption efficiency and ultimately the fate of contaminants in the environment. It should be further explored from both environmental and engineering aspects. Moreover, to our knowledge, impact of morphology and particle size of magnetite on their desorption/regeneration capacity and metal recovery is still missing in literature. Therefore, present study was conducted to explore the adsorptive interactions of Pb and Cd with three kinds of magnetite having different particle sizes and surface area characteristics. Batch adsorption experiments were performed to determine the effect of various adsorption parameters such as equilibrium concentration, contact time, effect of pH, temperature and competitive adsorption behavior. Moreover, to determine the extent and nature of adsorption, experimental adsorption data was further analyzed via adsorption kinetics and isotherm modeling. Finally, desorption of metal ions was also evaluated to explore the potential practical use of regenerated magnetites.

2. Experimental section

2.1. Chemical reagents and magnetites

Lead nitrate $Pb(NO_3)_2$ and cadmium nitrate $Cd(NO_3)_2$, ferrous sulfate heptahydrate ($FeSO_4.7H_2O$), ferrous chloride tetra hydrate ($FeCl_2.4H_2O$), and ferric chloride hexahydrate ($FeCl_3.6H_2O$), hydrochloric acid (HCl) and sodium chloride (NaCl) were purchased from Sigma Aldrich.

For this study, three kinds of magnetite (M1, M2 and M3) were used. Among them, M1 and M2 were synthesized in the laboratory by transforming 2-line ferrihydrite and lepidocrocite (γ-FeOOH) into magnetites in the context of our previous studies (Usman et al., 2012), while M3 (micro-magnetite) was purchased from Prolabo. Summary of three magnetites is presented in Table 1 while detailed characterization is provided elsewhere (Usman et al., 2014).

2.2. Batch experiments

The batch type experiments were conducted by using Pb and Cd stock solutions (1000 mg/L) prepared from 99.5% $Pb(NO_3)_2$ and Cd $(NO_3)_2$. The required concentrations were achieved by diluting these stock solutions. The pH was controlled by dropwise addition of NaOH or HCl. The metal ions adsorption experiments were carried out against various operational parameters such as pH (3–9), reaction time (5 min, 30 min, 1 h, 3 h, 6 h, and 24 h), initial solution concentration (20–170 mg/L) and temperature variations (15–45 °C) at pH (6.0) with constant sorbent dose of 4 g/L. The competitive adsorption behavior of both metals (Pb and Cd) was also investigated using 20 mg/L of each metal over a period of 24 h. After the adsorption was completed, the samples were centrifuged and supernatant (about 10 mL) was withdrawn through 0.45 μm polypropylene syringe and was used to measure metal concentration by atomic absorption spectrophotometer (AAS, Analyst 400, Perkin, Elmer). The metal ions adsorption capacity and equilibrium adsorbed amount per adsorbent gram was measured through Equations (1) and (2).

$$\%\text{Removal} = \frac{C_0 - C_e}{C_0} \times 100 \quad (1)$$

$$q_e = \frac{C_0 - C_e}{M} \times V \quad (2)$$

Herein, C_e and C_o denote equilibrium and initial metal ion concentrations (mg/L), q_e (mg/g) were the metal ions adsorbed per unit gram (g) of tested adsorbent, M represents the total adsorbent mass (g), while V is solution volume (L).

2.3. Desorption analysis and particles regeneration

Regeneration potential of saturated adsorbents is a key factor to determine its possible practical applications. To evaluate the reusability of tested materials, adsorption/desorption analysis were conducted for the metal ions loaded adsorbents here. Desorption was studied using distilled water and under acidic conditions. Desorption in 50 mL centrifuge tube was equilibrated over a period of 24 h. After equilibration, samples were centrifuged, decanted and filtered through 0.45 μm propylene syringe. The desorbed concentration was measured through atomic adsorption spectrophotometer. The residual materials were separated and used for further adsorption experiment. The separated materials were named as reusable adsorbents. The reusable materials were dried at 105 °C over a period of 24 h before their use for next adsorption cycle.

The desorption performance (%) was calculated using Equation (3):

$$\text{Desorption percentage}(\%) = \frac{C^*V}{X^*m} \times 100 \quad (3)$$

where C (mg/L) denotes desorbed metal ions concentration, x (mg/g) represents the adsorbed capacity of metal ions loaded samples prior to desorption, m (g) represents the total mass of particle which is used in desorption analysis, while V (L) denotes the desorption solution volume.

2.4. Adsorption isotherm and kinetic models

Two important isotherms were selected to fit experimental data in this study, namely the Langmuir and Freundlich isotherm models. Clarification of Pb and Cd adsorption kinetics to all tested adsorbents was investigated by using Lagergren's Pseudo-first-order, Pseudo-

Table 1
Physico-chemical properties of tested adsorbents.

Magnetite Sample	Source of magnetite	Particle Size (nm)	Pore volume cm^3/g	SSA ($m^2\ g^{-1}$)	PZC
M1	Ferrihydrite derived	30 nm	0.44	103 ± 2	7.9
M2	Lepidocrocite derived	60 nm	0.17	25 ± 1	7.7
M3	Purchased from Prolabo	1.5 μm	0.02	1.7 ± 0.1	7.4

Note: SSA means Specific Surface area, PZC means Point of zero charge.

second-order (Gerente et al., 2007) and Intra particle diffusion (Morris and weber, 1962). Mathematical expression of kinetic models is given below as equations (4)–(7)

$$\frac{dq_t}{q_t} = K_1(q_e - q_t) \quad \text{(Pseudo first order model)} \quad (4)$$

$$\frac{dq_t}{q_t} = K_2(q_e - q_t)^2 \quad \text{(Pseudo second order model)} \quad (5)$$

$$\frac{dq_t}{q_t} = \alpha \exp(-\beta q * t) \quad \text{(Elovich mode)} \quad (6)$$

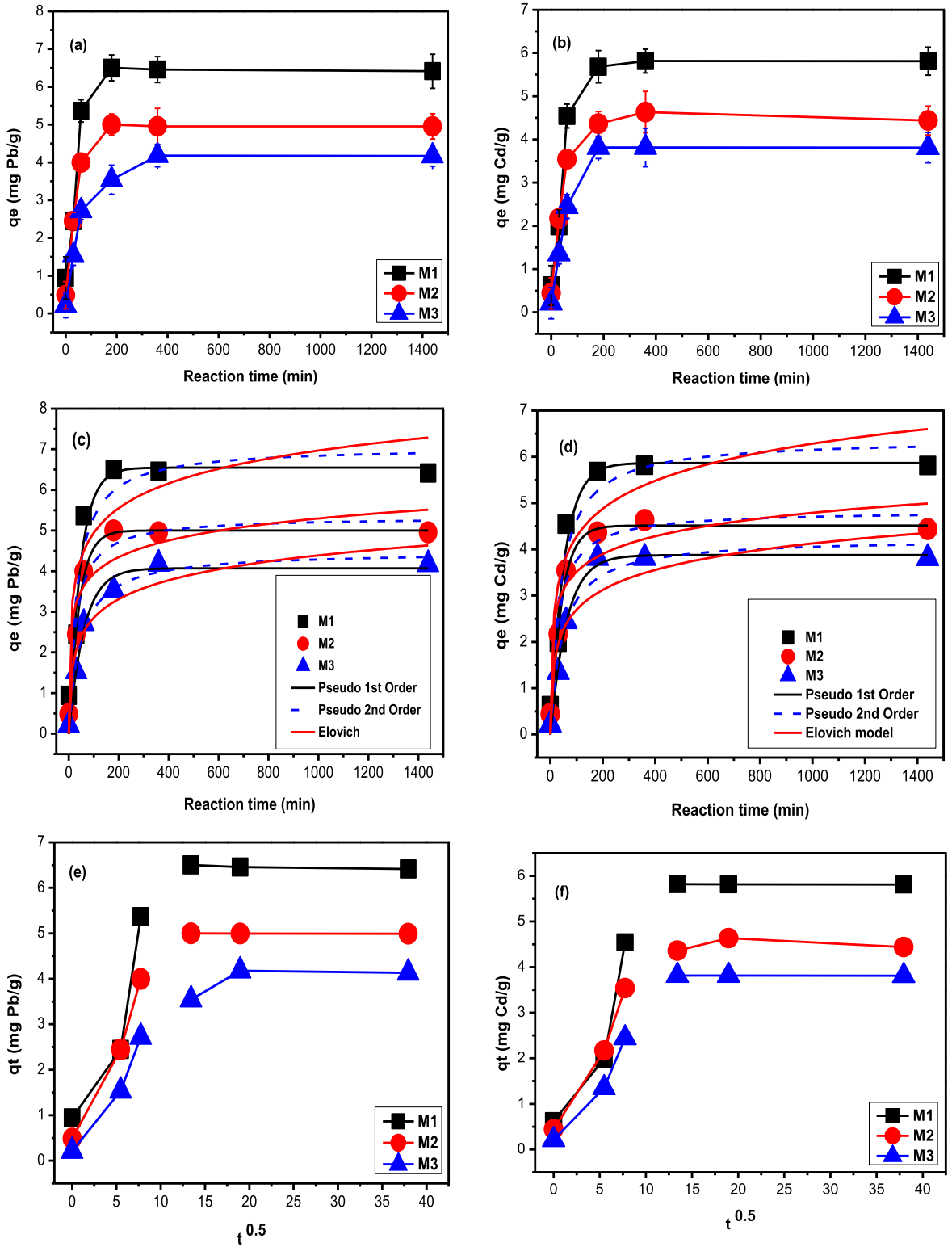

Fig. 1. Adsorption of Pb and Cd by using three kinds of magnetite (M1, M2 and M3) as a function of reaction time (24 h); solid = 4 g/L, Pb or Cd = 20 mg/L, pH = 6.0 ± 0.1; **(a, b).** Modling of Pb and Cd adsorption data by using various kintetic models **(c, d)** Pseudo 1st, 2nd order and Elovich model **(e, f)** Intraparticle.

$$q_t = K_d t^{1/2} + C \quad \text{(Intraparticle mode)} \tag{7}$$

where q_e and q_t (mg/g) are the metal ions adsorption capacity at equilibrium and time *t*, respectively, k_1 and k_2 are first and second order apparent rate constants, while α indicates initial adsorption coefficient mg/(g. h) and β indicates adsorption constant (g/mg).

The isotherm data was further evaluated by using Langmuir (Equation (8)) and Freundlich (Equation (9)).

$$q_e = \frac{KQC_e}{1 + KC_e} \quad \text{(Langmuir model)} \tag{8}$$

$$q_e = k_f C_e^{\,n} \quad \text{(Freundlich model)} \tag{9}$$

herein, K, K_f indicates Langmuir bonding term related to bonding energies (L/mg), Freundlich affinity coefficient ($L^n/mg^{n-1}g$) C_e (mg/L) stands for residual concentration, Q (mg/g) denotes optimum Langmuir adsorption capacity, β (L/mg) represent equilibrium constant, K_f and n are Freundlich constants.

3. Results and discussion

3.1. Adsorption characteristics

3.1.1. Adsorption kinetics

The effect of reaction time on metals adsorption by M1, M2, and M3 is presented in Fig. 1, which represents two phase kinetic adsorption behaviors. All tested adsorbents firstly exhibited a rapid metal adsorption. With an increase in reaction time, adsorption was dramatically increased, and saturation point was achieved at 180, 180, 360 min for M1, M2 and M3, respectively for Pb (Fig. 1a and b), and for Cd at 360 min for three magnetites. This could be correlated to the large number of available surface sites at initial phase of adsorption process which are saturated as adsorption proceeds. Owing to the existence of relatively larger driving force between metal ions and solid surface sites, higher metal uptake was observed (curve was more vertical at initial adsorption stage) in a shorter period of time to reach equilibrium for all tested adsorbents. This initial adsorption stage was generally known by external or instantaneous surface adsorption. Thereafter, the driving forces became weaker and the adsorption rate of metal ions slowed down. Overall, observed equilibrium point was smaller than many of the reported studies (Ozdes et al., 2011).

Furthermore, the metal ions adsorption properties for all tested adsorbents followed the order M1 > M2 > M3, similar to that for the equilibrium point. The overall experimental data confirmed that particle size and surface area characteristics dictate the adsorption capacity of adsorbents. Owing to the nanosized particles and higher surface area, nano-magnetites could offer considerable surface-active site for efficient metal ions adsorption rather than that by micro-sized particles.

The kinetic models were used for the simulation of Pb and Cd adsorption data for all tested adsorbents. The non-linearized profile parameters and calculated regression values are reported in Table 2. Obtained data showed poor fitting of pseudo-second order and Elovich model to describe the experimental data. The range of R^2 values of pseudo second order and Elovich model for Pb and Cd were 0.75–0.94 for all tested adsorbents. The estimated q_e, k_2 and R^2 are presented in Table 2. However, the metal ions adsorption data for M2 and M3 was better fitted to pseudo-first order model with (R^2 = 0.997–0.999) rather than pseudo-second order (R^2 = 0.91–0.93) and intraparticle diffusion (R^2 = 0.51, 0.65). Our results contradict with certain previous reports where pseudo-second order model was found to be the best fit for metal ions adsorption over iron-oxides (magnetite) surface sites (Wang et al., 2012; Bagbi et al., 2016). Depending upon correlation coefficient values (>90), the M1 adsorption experimental data showed better fitting to both pseudo-first and second order model for both metals (Pb & Cd) (Gerente et al., 2007). At the edge of saturation point, the adsorption process could be further controlled via other secondary pathways. They may include; pore or film diffusion that may possibly preside over the physical metal ions transfer from bulk liquid to the solid surface interface (Rehman et al., 2013). Overall, initial quick metal ions uptake onto magnetites surface sites via film diffusion (external mass transfer) is followed by a pore diffusion mechanism (intraparticle) until the equilibrium point is reached. The role of pore diffusion was further investigated by evaluating the experimental kinetic data by intra-particle diffusion model (Fig. 1 and Table 2). The plot between Pb and Cd uptake *vs* $t^{1/2}$ indicates a bilinear trend, i.e. two straight lines (Fig. 1g and h). The first increasing trend line clearly indicates the mesopores and macrospores diffusion of adsorbed ions, while that of other line indicates microspore diffusion of adsorbed ions onto tested adsorbents. The experimental data between q_t vs $t^{1/2}$ at the initial stage show curvature, which is generally ascribed to the external and instantaneous mass transfer or boundary layer diffusion effects. This initial linear trend can be associated to the involvement of film diffusion. The intercept value obtained from linear portions of the plots back to the y-axis shows the measurement of the boundary layer thickness. The straight lines deviation from origin may be due to rate of mass transfer difference at initial and final stages of adsorption (Crank, 1965; Allen et al., 1989). Moreover, straight line deviation, which is not passing through the origin ($C \neq 0$), further indicates the non-significant contribution of intra-particle diffusion as a rate controlling step, which further suggests that metal ions adsorption was mainly governed mutually (film and intra-particle). This trend in adsorption kinetic intraparticle model indicates a significant contribution of two or more processes to facilitate the adsorption of metal ions species onto tested adsorbents surface sites. The q_t versus $t^{1/2}$ slope refers to the rate parameter characteristic of adsorption rate in the region wherever intra-particle diffusion is not the rate controlling step (McKay et al., 1980).

3.1.2. Adsorption equilibrium

The results of the effect of metal ions concentration for all tested adsorbents (M1, M2, and M3) are presented in Fig. 2 and Table 3. These results indicate that an increase in initial concentration of metal ions favors their adsorption (C_o–C_e). The highest adsorption capacities were 38 ± 1.04 mg/g (M1), 33 ± 1.21 mg/g (M2), and 26 ± 0.98 mg/g (M3), at highest concentration (170 mg/L). Meanwhile, the percentage removal rate indicated a tendency to decrease. Decreases in metal ion removal with an increase in initial metal ion solution concentration

Table 2
The profile parameter and calculated modeled based values for Pb and Cd adsorption onto original magnetites (M1, M2 and M3).

Material	Pseudo 1st order				Pseudo 2nd order			Elovich			Intraparticle		
	Q_{exp}	qe (mg/g)	K_1 (1/h)	R^2	q_e (mg/g)	K_2 (g/mg/h)	R^2	α (mg/g)	β (g/mg)	R^2	K_d (mg/g/min^{-1})	C (mg/g)	R^2
M1	6.50	6.54	0.021	0.904	7.06	0.004	0.914	2.38	1.13	0.752	0.34	7.80	0.656
M2	5.03	5.00	0.024	0.978	5.34	0.007	0.929	4.57	1.69	0.861	0.44	10.0	0.530
M3	4.21	4.07	0.016	0.980	4.48	0.004	0.939	0.46	1.48	0.911	0.71	10.6	0.510
Cd													
M1	5.89	5.86	0.019	0.919	6.38	0.004	0.929	1.16	1.14	0.798	0.42	8.10	0.595
M2	4.38	4.51	0.023	0.977	4.83	0.007	0.933	3.18	1.80	0.863	0.50	11.1	0.543
M3	3.82	3.87	0.016	0.989	4.23	0.005	0.921	0.45	1.59	0.851	0.74	11.4	0.533

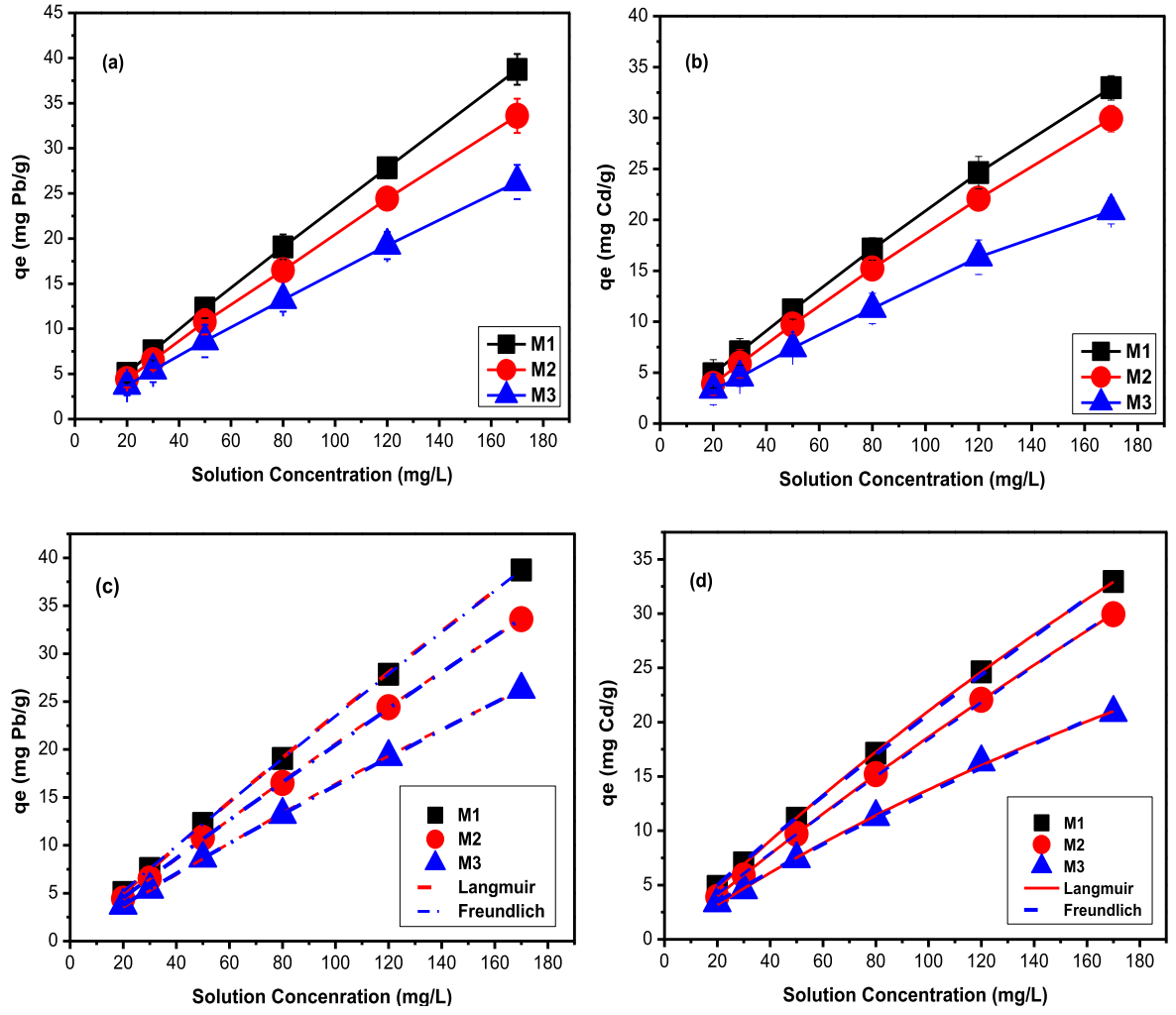

Fig. 2. Adsorption of Pb and Cd using three kinds of magnetite (M1, M2 and M3) as a function of various initial solution concentration (20–170 mg/L), reaction time = 24 h, solid = 4 g/L, pH = 6.0 ± 0.1 **(a, b).** Modling of isothrem adsorption data by using Langmuir and Freundlich model**(c, d).**

Table 3
The profiles parameters and calculated Langmuir and Freundlich values for Pb and Cd adsorption.

Material	Langmuir			Freundlich		
	Q ($mg.g^{-1}$)	*K* (L/mg)	R_L^2	K_F ($L^n/(mg^{(n-1)}.g)$	n	R_F^2
Pb- M1	408.14	0.00061	0.999	0.30	0.94	0.999
Pb- M2	331.40	0.00066	0.999	0.27	0.93	0.999
Pb- M3	178.47	0.00101	0.999	0.25	0.91	0.959
Cd-M1	228.05	0.0014	0.999	0.35	0.88	0.999
Cd-M2	170.86	0.0008	0.999	0.26	0.92	0.999
Cd-M3	83.49	0.0019	0.998	0.26	0.85	0.952

were 72–65% (M1), 63-56% (M2), and 53-44% (M3). It can be closely associated to the fixed amount of adsorbent dose (fixed surface binding sites) against increasing concentration (high metal ions availability in solution). Because, with increase in solution concentration, due to constant adsorbent dosage the amount of surface sites remains constant or lower as compared to increasing metal ions in solution. It could indicate a decrease in metal ions percentage removal rather than adsorption capacity (C_o–C_e). Initial concentration makes the required driving forces available to prevail over the resistance to the mass transfer of metal ions between bulk liquid to solid phase. On the other hand, this could be better associated to higher gradient between adsorbate/adsorbent interface caused by the existence of larger driving force by an increase in solution concentration. It promotes interaction between adsorbent/adsorbate with high adsorption capacity (C_o–C_e) against fixed adsorbent dose (M) due to high mass transfer, thereby resulting into higher adsorption performance (Q_e). Because, at low initial metal ions concentration, the more surface binding sites were available and many of them were vacant and thus these vacant surface binding sites were covered with an increase in adsorbate concentration. The incremental increase in adsorption capacity by increasing adsorbate concentration could be illustrated via Equation (2).

Adsorption isotherm is imperative for the optimization of studied materials. The equilibrium relationship between adsorbate and adsorbent interface (ratio between amounts of metal ions adsorbed to its residual amount in liquid phase at equilibrium stage), are usually explained by adsorption isotherm. Therefore, the isotherm data was further evaluated by applying above-mentioned Freundlich and Langmuir equations. In order to describe the Langmuir model, it is important to determine the separation factor (Weber and Chakravorti, 1974), as essential characteristics of Langmuir isotherm can be expressed in terms of a dimensionless constant called the separation factor.

$$R_L = (1 / [1 + K_L Co) \quad (10)$$

The better fitting of Langmuir model explains that adsorbate species interaction mainly depends upon calculated separation factor regression values (R^2), which represent favorable adsorption process (when $0 < R_L < 1$), unfavorable ($R_L > 1$), linear adsorption ($R_L = 1$) and irreversible

adsorption ($R_L = 0$). The better fitting of Langmuir model for all tested adsorbents clearly indicates the feasibility of magnetite as an adsorbent. Thus, the calculated Langmuir adsorption capacity was higher than that of previously reported fly ash (0.22 mmol/g) (Papandreou et al., 2011) and chitosan-tripolyphosphate (57.33 mg/g) adsorbents for Pb and Cd ions (Ngah and Fatinathan, 2010). The Freundlich model also indicated the better fitting of isotherm metal ions adsorption data obtained from nano-magnetites. Furthermore, it indicates that the relationship between metal ions and nano-magnetites samples was primarily better simulated via both Langmuir and Freundlich models as reported in literature (Weijiang et al., 2017).

3.1.3. Effect of temperature

To investigate the effect of temperature, metal ion adsorption was tested at varied temperature of 288.15–328.15 K. The results are presented in Fig. 3. The metal ions adsorption generally increased with an increase in temperature. The maximum metal ion adsorptions were achieved at 328.15 K for all tested adsorbents. Optimum values for Pb and Cd were 7.72 ± 0.2, 7.34 ± 0.34, 6.14 ± 0.47 and 7.60 ± 0.26, 7.25 ± 0.47, 6.03 ± 0.44 mg/g in the order of M1 > M2 > M3. Increase in temperature is considered favorable for the pore diffusion of unadsorbed metal ion species onto the tested adsorbents because of decreasing solution viscosity and high free energy availability, which boost up the adsorption at high temperature (Nassar, 2010). Moreover, at higher temperature, the diffusion of adsorbate (metal ions) from external laminar layer into the micro-pores of tested adsorbent increases between adsorbate and adsorbent surface functional groups.

3.1.4. Effect of solution pH

The solution pH is known to affect metals ion solubility, their ionization degree and adsorbent's surface characteristics. The results of the metal ions (Pb & Cd) adsorption onto tested adsorbents are presented in Fig. 4a and b. The overall findings showed that at initial pH 3, the Pb adsorption was 1.35 ± 0.15, 1.12 ± 0.20, 0.71 ± 0.11 mg/g, which increased up to 6.73 ± 0.20, 5.86 ± 0.18, 4.72 ± 0.31 mg/g at pH 6 for all tested adsorbents. Similar trend of increasing adsorption rate with pH from 3 to 6 was also observed for Cd adsorption onto all tested adsorbents, where adsorption was maximum at pH 6 (6.68 ± 0.29, 5.31 ± 0.30, 4.25 ± 0.19 mg/g for M1, M2 and M3, respectively). Similar findings regarding increase in Pb and Cd adsorption up to pH 6 and 5.5 are also available in literature (Ren et al., 2012; Weijiang et al., 2017). In adsorption, pH affects protonation of surface groups and speciation of metal ions in the solution (Repo et al., 2010). The low adsorption of both Pb and Cd in acidic medium was attributed to the competition between positively charged metal ion species and protons (H^+) ions onto tested adsorbents surfaces. Moreover, in lower pH range, there are more positively charged surface active sites and repulsive forces become dominant between adsorbent/adsorbate interfaces and thereby reduce the adsorption capacity at pH ˂ 6 (Singla and Chawla, 2001; Tang et al., 2009). As reported by Cornell and Schwertmann (2003), Fe_3O_4 may further produce Fe(II) and its hydrolysis products in the form of ($FeOH^+$), $Fe(OH)_{2^-}$, and $Fe(OH)_3$) mainly depending upon solution pH. Herein, the different magnetites surface sites (PZC) presented in Table 1 indicate that dominant surface functional groups would be $(FeOH)_{2^-}$ at pH < PZC (Cornell and Schwertmann, 2003). The incremental increase in metal adsorption with an increase in pH up to 6, may be due to lower competition of positively charged metal ions and the protons (Paulino et al., 2008). Because, increase in pH value from 3 to 6 enhances the adsorbent surface sited protonation, and thus yields more negatively-charged adsorbent surface sites. These negative surface charges are responsible for incremental increase in attractive forces between adsorbent/adsorbate to attain maximum adsorption capacity only up to pH 6 (Cheng et al., 2012). The pH dependent maximum Pb adsorption onto γ-Fe_2O_3 and Fe_3O_4 was achieved at pH ≥ 5.5 in the presence of competitive ions (Cd) (Roonasi and Holmgren, 2009). When the solution pH increased beyond 6, adsorption started to decrease. It might be associated to the precipitation of metal with an increase in pH, which decreased their adsorption as observed previously (Farghali et al., 2013).

3.1.5. Competitive adsorption of metals

The results of competitive adsorption behavior of both Pb and Cd ions for all tested adsorbents are presented in Fig. 4c and d. The overall adsorption results show that equilibrium point for both species with optimum adsorption rate (5.62 ± 0.12, 5.18 ± 0.11, 3.86 ± 0.15 (Pb) and 4.41 ± 0.13, 3.53 ± 0.15, 2.87 ± 0.12 mg/g (Cd)) for M1, M2, and M3, respectively) was obtained at 180 min. Thereafter, the adsorption rate for both metal ions tended to decrease as compared to the mono-metallic systems at constant ionic strength due to their competition for surface-active adsorption sites as reported elsewhere (Badruddoza et al., 2013). It was also observed that adsorption of Pb was higher than that of Cd ions for three adsorbents. It should be noted that the competitive adsorption aptitude differs from metal to metal, mainly depending upon several factors i.e. ion charges, molecular mass, metal hydration energy, and hydrated ionic radius (Qin et al., 2006). In dual or multi-metal systems, metals having greater affinity to adsorbents can displace the

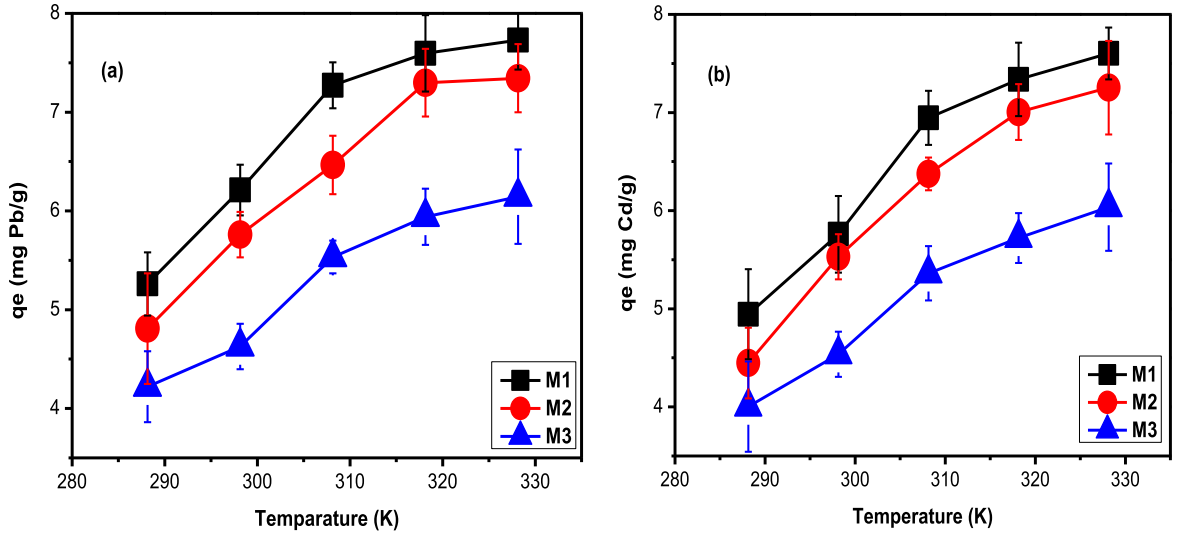

Fig. 3. Adsorption of Pb (a) and Cd (b) using three kinds of magnetite (M1, M2 and M3) as a function of temperature (288.15–328.15 K) at time = 24 h, solid = 4 g/L, Pb or Cd = 20 mg/L, pH = 6.0 ± 0.1.

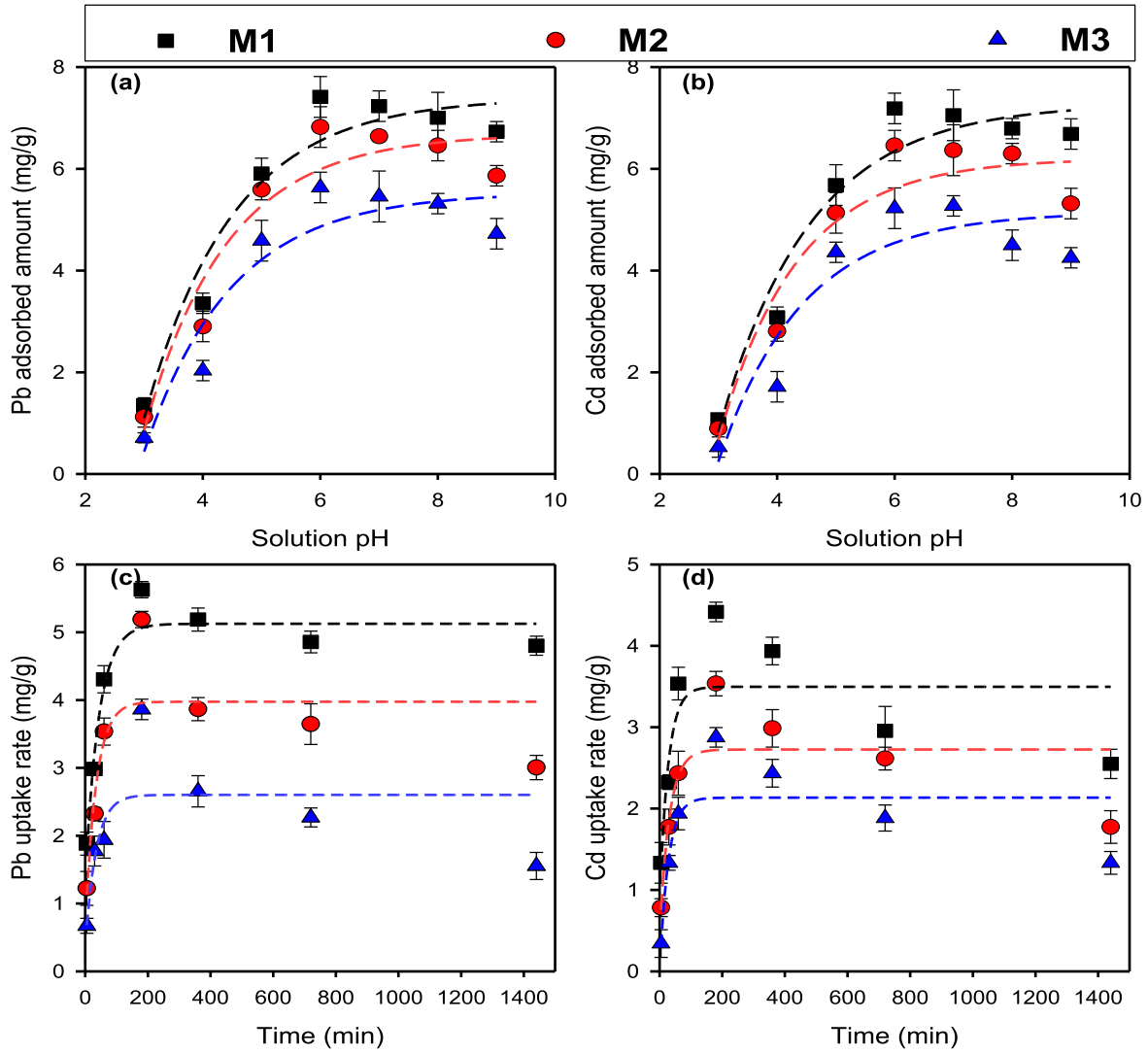

Fig. 4. **(a, b):** Effect of pH on Pb and Cd adsorption by using three kinds of magnetite (M1, M2 and M3) at pH = 3–9, reaction time = 24 h, solid = 4 g/L, Pb or Cd = 20 mg/L **(c,d)**: Competitive adsorption behavior of Pb and Cd adsorption in multi-metal solution at reaction time = 24 h, solid = 4 g/L, Pb & Cd = 20 mg/L of each, pH = 6.0 ± 0.1.

metals with weaker affinity and thus their adsorption will be favored (Qin et al., 2006). The similar sequence in multi-metal solution (Pb > Cd) onto different tested adsorbents surfaces, comprising –COOH and –OH functional groups has also been reported in literature (Qin et al., 2006). Similar to our study, Hur et al. (2015) also observed higher affinity of Pb for adsorption sites than Cu and Cd and suggested that it could be associated to the distribution of specific surface adsorption sites for each metal. That can be closely associated with high hydrated radius and lowest electronegativity of adsorbed metals (Hur et al., 2015).

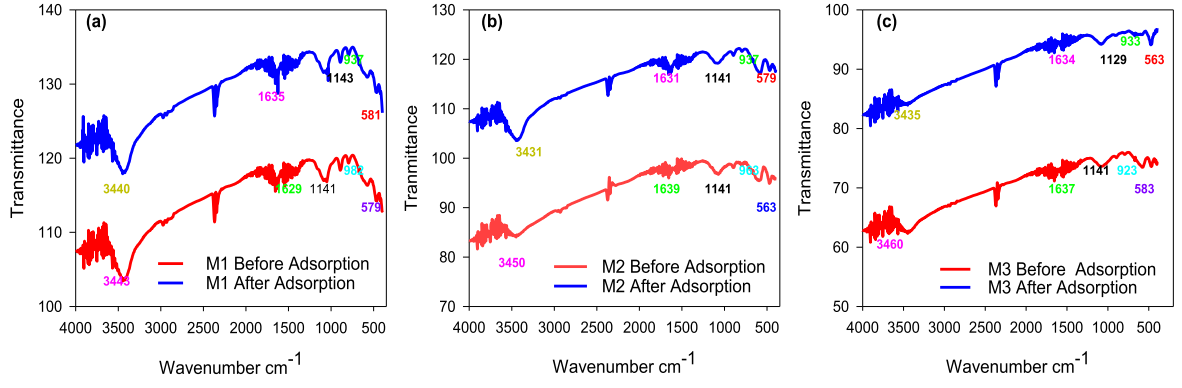

Fig. 5. FTIR spectrum of M1 (a), M2 (b) and M3 (c) before and after Pb and Cd adsorption.

3.1.6. FTIR data interpretation

The FTIR spectra of all tested adsorbents (M1, M2 and M3) are presented in Fig. 5. The corresponding peaks to various surface functional groups before and after metal ions adsorption are compared. The corresponding peak at 563, 573, and 581 indicate the Fe–O band vibrations at tetrahedral sites for all tested adsorbents. After adsorption, these bands shifted to 593 and 591 for Pb and Cd ions, respectively. Peaks at 1635, 1637 and 1639 indicate the stretching vibration of C=C groups and OH stretching mode of water molecule (Rezaei et al., 2011). The peaks exist at 3439, 3443, 3451 for adsorbed water and indicates hydroxyl groups (-OH) during material synthesis. The broad peaks around 923–1143 are attributed to the bonded hydroxyl group onto surfaces of metal oxide (Alvarez Ayuso et al., 2007). After adsorption, these peaks shift to 978, 961, 921 and 1123, 1139, 1152. All these shifts clearly indicate that involvement of possible adsorption process via surface Fe–O, hydroxyl, and carboxyl groups.

3.2. Desorption performance and particle reusability

Metal ions desorption from saturated particles was investigated by using distilled water and acidic solution through Equation (3) and obtained results are presented in Fig. 6(a and b). The metal ions desorption in distilled water for Pb and Cd was found to be almost 44, 38, 37 and 41, 36, 34% by M2, M1 and M3, respectively. On the other hand, desorption in acidic environment followed the order M2 > M3 > M1, with maximum desorption percentage 91, 87, 82 and 92, 89, 82% for Pb and Cd, respectively. The better desorption in acidic environment can be attributed to higher H^+ ions leading to higher positively charged surface sites (Ren et al., 2012). Moreover, observed incomplete regeneration might be caused by chemical reaction (i.e. oxidation and passivation of magnetite) during adsorption/desorption cycles (Javadian et al., 2015). Conversely, the slightly lower desorption percentage of M1 might be associated to its porous nature arising from its parent mineral, ferrihydrite (Usman et al., 2012). It further indicates that the adsorbed metal ions have stronger bond with fine pores of tested adsorbent, which could lead to a difficult desorption even in strong acidic solution. It further emphasizes the need to investigate the impact of time onto the nature of adsorbents for subsequent adsorption/desorption cycles. Taking into the account the desorption from all tested adsorbents, M2 achieved more desorption (%) that can be associated to its higher stability.

Moreover, adsorption potential of regenerated adsorbents (after 1st adsorption cycle) was comparable to that of freshly-prepared adsorbents, whereas about 10–20% decrease in adsorption efficiency was observed after six adsorption/desorption cycles (Fig. 6). This considerable adsorption performance with consecutive regeneration cycles indicates the breakdown of large bulks into small ones, which led to the exposure of more surface binding sites for adsorption (Ren et al., 2012). On the other hand, slightly lower adsorption percentage of reused adsorbents can be attributed to the existence of already occupied surface active sites or the loss of porosity. Many researchers have reported the similar phenomenon of decreased adsorption performance in reusability tests, which was correlated to the erosion of adsorbent surface sites

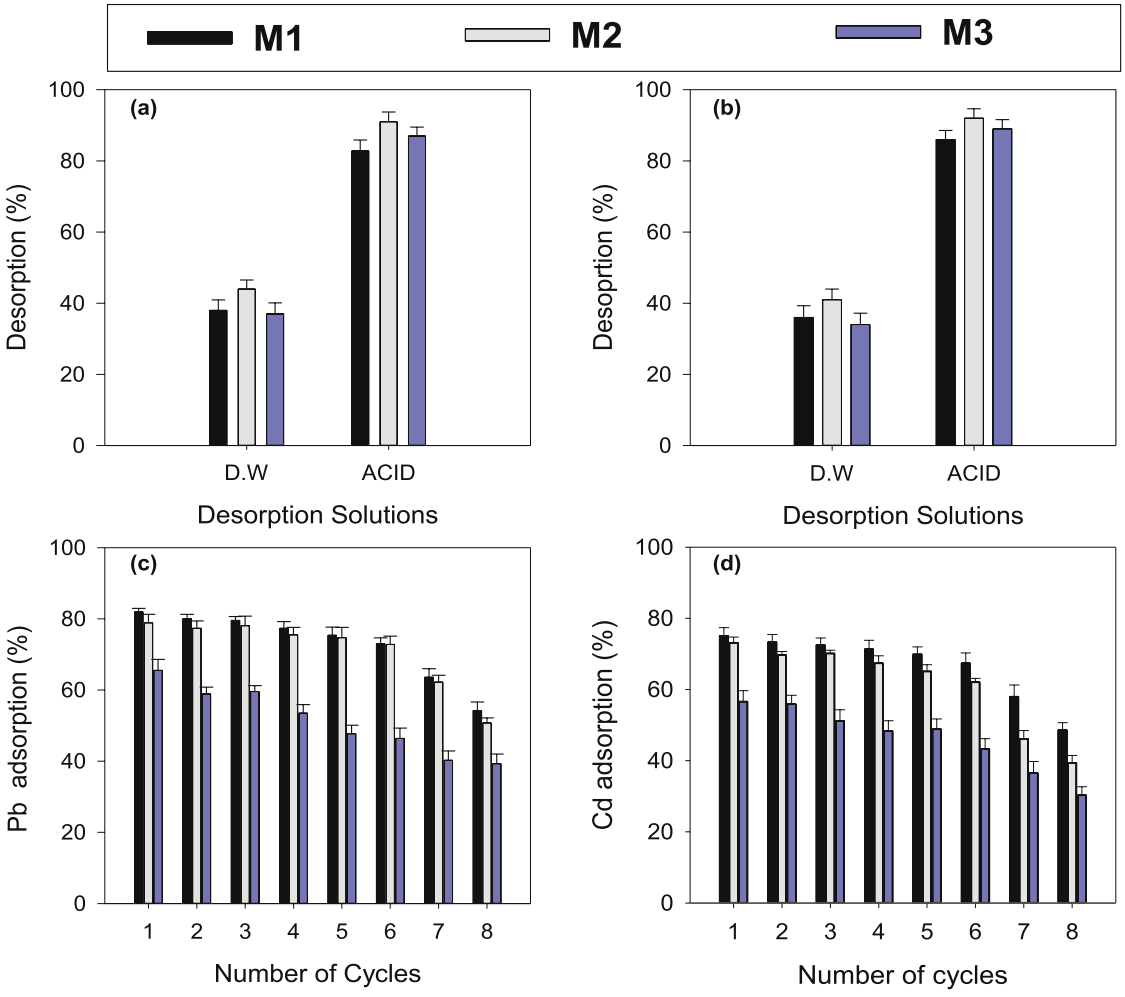

Fig. 6. Desorption performance (in distilled water (D.W) and acid (0.1 M H_2SO_4) and subsequent adsorption cycles of three magnetites (M1, M2 and M3) for Pb **(a, c),** and Cd **(b, d),** respectively (reaction time = 24 h, solid = 2 g/L).

leading to the loss of adsorbent porosity during metal ion adsorption and nutrient recovery analysis onto iron oxides and biochar-based adsorbents (Nassar, 2010; Kizito et al., 2017; Ajmal et al., 2018). Similarly, slight decrease in adsorption performance of zeolite based geopolymers adsorbent for Cd removal from aqueous solution has already been reported (Javadian et al., 2015). Taking into the account of all the desorption data; it is evident that M1 and M2 showed better desorption efficiency than M3. It is important to note that regeneration of saturated adsorbents can significantly reduce the treatment cost as it can be an expensive step during adsorption process accounting for about 75% of the total maintenance and operating cost (Inglezakis and Poulopoulos, 2006). However, consecutive regeneration of magnetite has been noted with considerable adsorption performance in present study.

4. Conclusions

Present study reports superior metal ions adsorption by nano-magnetites (M1 and M2) than that by micro-magnetite (M3) (M1 > M2 > M3) thereby, demonstrating the prominent role of their physico-chemical characteristics (particle size and surface area) in pollutant adsorption and immobilization. The kinetic data was better fitted to pseudo-first order model, while Langmuir and Freundlich models seem to be best fit for nano-magnetites adsorption data rather than micro-magnetite, where monolayer (Langmuir) was dominant. Electrostatic attraction and surface precipitation interaction via external mass transfer between bulk liquid to solid surface interface and surface functional groups (hydroxyl and carboxyl) were found as potential adsorption pathways rather than intraparticle diffusion. Experiments in single and binary metal contamination systems revealed competitive adsorption with affinity order of Pb > Cd. Thus, these findings demonstrate the effect of particle size and surface properties of a mineral in dictating the adsorption/desorption capacity, which has strong implications in understanding the fate and immobilization of metals in natural and engineered settings.

Declaration of competing interest

The authors declare that they have no known competing financial interests or personal relationships that could have appeared to influence the work reported in this paper.

CRediT authorship contribution statement

Zeeshan Ajmal: Data curation, Methodology, Investigation, Writing - original draft. **Muhammad Usman:** Conceptualization, Writing - review & editing, Funding acquisition. **Ioannis Anastopoulos:** Formal analysis, Methodology, Writing - review & editing. **Abdul Qadeer:** Data curation, Investigation. **Runliang Zhu:** Writing - review & editing. **Abdul Wakeel:** Supervision, Writing - review & editing. **Renjie Dong:** Supervision, Writing - review & editing.

Acknowledgment

Financial support of this research has been provided by Grand Challenges Canada–Stars in Global Health (Grant No.: GCC- 0242-01).

References

Ajmal, Z., Muhmood, A., Usman, M., Kizito, S., Lu, J., Dong, R., Wu, S., 2018. Phosphate removal from aqueous solution using iron oxides: adsorption, desorption and regeneration characteristics. J. Colloid Interface Sci. 528, 145–155.
Ajmal, Z., Muhmood, A., Dong, R., Wu, S., 2020. Probing the efficiency of magnetically modified biomass-derived biochar for efffective phosphate removal. J. Environ. Manag. 253, 109730.
Allen, S.J., McKay, G., Khader, K.Y.H., 1989. Intraparticle diffusion of a basic dye during adsorption onto sphagnum peat. Environ. Pollut. 56, 39–50.
Alvarez Ayuso, E., Garcia-Sanchez, A., Querol, X., 2007. Adsorption of Cr(VI) from synthetic solutions and electroplating wastewaters on amorphous aluminium oxide. J. Hazard Mater. 142, 191–198.
Badruddoza, A.Z.M., Shawon, Z.B.Z., Tay, W.J.D., Hidajat, K., Uddin, M.S., 2013. Fe_3O_4/cyclodextrin polymer nanocomposites for selective heavy metals removal from industrial wastewater. Carbohydr. Polym. 91, 322–332.
Bagbi, Y., Sarswat, A., Mohan, D., Pandey, A., Solanki, P.R., 2016. Lead (Pb^{2+}) adsorption by monodispersed magnetite nanoparticles: surface analysis and effects of solution chemistry. J. Environ. Chem. Eng. 4, 4237–4247.
Cheng, Z., Tan, A.L.K., Tao, Y., Shan, D., Ting, K.E., Yin, X.J., 2012. Synthesis and characterization of iron oxide nanoparticles and applications in the removal of heavy metals from industrial wastewater. Int. J. Photoenergy.
Cornell, R.M., Schwertmann, U., 2003. The Iron Oxides: Structure, Properties, Reactions, Occurrence and Uses, second ed. Wiley-VCH.
Crank, J., 1965. The Mathematics of Diffusion. Oxford Clarendon Press, London, p. 84.
Farghali, A.A., Bahgat, M., Enaiet Allah, A., Khedr, M.H., 2013. Adsorption of Pb(II) ions from aqueous solutions using copper oxide nanostructures. Beni-Suef Uni. J. Basic Appl. Sci. 2, 61–71.
Fu, F., Wang, Q., 2011. Removal of heavy metal ions from wastewaters: a review. J. Environ. Manag. 92, 407–418.
Fu, H., He, H., Usman, M., Chen, Q., Laipan, M., Yang, Y., Zhu, R., Cai, L., 2019. Facile synthesis of Al/Fe bimetallic (oxyhydr)oxide-coated magnetite for efficient removal of fluoride from water. Environ. Technol. 1–12.
Gerente, C., Lee, V.K.C., Cloirec, P.L., McKay, G., 2007. Application of chitosan for the removal of metals from wastewaters by adsorption—mechanisms and models review. Crit. Rev. Environ. Sci. Technol. 37, 41–127.
Hamid, Y., Tang, L., Hussain, B., Usman, M., Gurajala, H.K., Rashid, M.S., He, Z., Yang, X., 2019a. Efficiency of lime, biochar, Fe containing biochar and composite amendments for Cd and Pb immobilization in a co-contaminated alluvial soil. Environ. Pollut. 113609.
Hamid, Y., Tang, L., Sohail, M.I., Cao, X., Hussain, B., Aziz, M.Z., Usman, M., He, Z.-l., Yang, X., 2019b. An explanation of soil amendments to reduce cadmium phytoavailability and transfer to food chain. Sci. Total Environ. 660, 80–96.
Hamid, Y., Tang, L., Sohail, M.I., Cao, X., Hussain, B., Aziz, M.Z., Usman, M., He, Z.l., Yang, X., 2019c. An explanation of soil amendments to reduce cadmium phytoavailability and transfer to food chain. Sci. Total Environ. 660, 80–96.
Hamid, Y., Tang, L., Hussain, B., Usman, M., Lin, Q., Rashid, M.S., He, Z., Yang, X., 2020. Organic soil additives for the remediation of cadmium contaminated soils and their impact on the soil-plant system: a review. Sci. Total Environ. 707, 136121.
Hur, J., Shin, J., Yoo, J., Seo, Y.S., 2015. Competitive adsorption of metals onto magnetic graphene oxide: comparison with other carbonaceous adsorbents. Sci. World J. 2015.
Inglezakis, V.J., Poulopoulos, S.G., 2006. Adsorption, Ion Exchange and Catalysis: Design of Operations and Environmental Applications, first ed. Elsevier, UK.
Javadian, H., Ghorbani, F., Tayebi, H.-a., Asl, S.H., 2015. Study of the adsorption of Cd (II) from aqueous solution using zeolite-based geopolymer, synthesized from coal fly ash; kinetic, isotherm and thermodynamic studies. Arabian J. Chem. 8, 837–849.
Kizito, S., Luo, H., Wu, S., Ajmal, Z., Lv, T., Dong, R., 2017. Phosphate recovery from liquid fraction of anaerobic digestate using four slow pyrolyzed biochars: dynamics of adsorption, desorption and regeneration. J. Environ. Manag. 201, 260–267.
McKay, G., Otterburn, M.S., Sweeney, A.G., 1980. The removal of colour from effluent using various adsorbents—III. Silica: rate processes. Water Res. 14, 15–20.
Morris, J.C., Weber, W.J., 1962. Preliminary appraisal of advanced waste treatment processes. Int. Conf. Adv. Water Pollut. Res. 2, 231–241.
Murtaza, G., Yawar, U., Niazi, N.K., Muhammad, U., Tajammal, H., 2017. Bioaccumulation of potentially toxic elements in cereal and legume crops: a review. Clean 45, 1700548-1700548.
Nassar, N.N., 2010. Rapid removal and recovery of Pb(II) from wastewater by magnetic nanoadsorbents. J. Hazard Mater. 184, 538–546.
Ngah, W.S.W., Fatinathan, S., 2010. Adsorption characterization of Pb(II) and Cu(II) ions onto chitosan-tripolyphosphate beads: kinetic, equilibrium and thermodynamic studies. J. Environ. Manag. 91, 958–969.
Ozdes, D., Duran, C., Senturk, H.B., 2011. Adsorptive removal of Cd(II) and Pb(II) ions from aqueous solutions by using Turkish illitic clay. J. Environ. Manag. 92, 3082–3090.
Papandreou, A.D., Stournaras, C.J., Panias, D., Paspaliaris, I., 2011. Adsorption of Pb(II), Zn(II) and Cr(III) on coal fly ash porous pellets. Miner. Eng. 24, 1495–1501.
Parsons, J.G., Hernandez, J., Gonzalez, C.M., Gardea Torresdey, J.L., 2014. Sorption of Cr(III) and Cr(VI) to high and low pressure synthetic nano-magnetite (Fe_3O_4) particles. Chem. Eng. J. 254, 171–180.
Paulino, A.T., Santos, L.B., Nozaki, J., 2008. Removal of Pb^{2+}, Cu^{2+}, and Fe^{3+} from battery manufacture wastewater by chitosan produced from silkworm chrysalides as a low cost adsorbent. React. Funct. Polym. 68, 634–642.
Qin, F., Wen, B., Shan, X.Q., Xie, Y.N., Liu, T., Zhang, S.Z., Khan, S.U., 2006. Mechanisms of competitive adsorption of Pb, Cu, and Cd on peat. Environ. Pollut. 144, 669–680.
Rehman, M.S.U., Munir, M., Ashfaq, M., Rashid, N., Nazar, M.F., Danish, M., Han, J.-I., 2013. Adsorption of Brilliant Green dye from aqueous solution onto red clay. Chem. Eng. J. 228, 54–62.
Ren, Y., Li, N., Feng, J., Luan, T., Wen, Q., Li, Z., Zhang, M., 2012. Adsorption of Pb(II) and Cu(II) from aqueous solution on magnetic porous ferrospinel $MnFe_2O_4$. J. Colloid Interface Sci. 367, 415–421.
Repo, E., Warchol, J.K., Kurniawan, T.A., Sillanpää, M.E.T., 2010. Adsorption of Co(II) and Ni(II) by EDTA- and/or DTPA-modified chitosan: kinetic and equilibrium modeling. Chem. Eng. J. 161, 73–82.

Rezaei, M., Khajenoori, M., Nematollahi, B., 2011. Synthesis of high surface area nanocrystalline MgO by pluronic P123 triblock copolymer surfactant. Powder Technol. 205, 112–116.

Roonasi, P., Holmgren, A., 2009. An ATR-FTIR study of sulphate sorption on magnetite; rate of adsorption, surface speciation, and effect of calcium ions. J. Colloid Interface Sci. 333, 27–32.

Singer, D.M., Chatman, S.M., Ilton, E.S., Rosso, K.M., Banfield, J.F., Waychunas, G.A., 2012. Identification of simultaneous U(VI) sorption complexes and U(IV) nanoprecipitates on the magnetite (111) surface. Environ. Sci. Technol. 46, 3811–3820.

Singla, A., Chawla, M., 2001. Chitosan: some pharmaceutical and biological aspects an update. J. Pharm. Pharmacol. 53, 1047–1067.

Tang, Q., Sun, X., Li, Q., Wu, J., Lin, J., 2009. Synthesis of polyacrylate/polyethylene glycol interpenetrating network hydrogel and its sorption of heavy-metal ions. Sci. Technol. Adv. Mater. 10, 015002.

Usman, M., Abdelmoula, M., Hanna, K., Gregoire, B., Faure, P., Ruby, C., 2012. Fe^{II} induced mineralogical transformations of ferric oxyhydroxides into magnetite of variable stoichiometry and morphology. J. Solid State Chem. 194, 328–335.

Usman, M., Martin, S., Cimetiere, N., Giraudet, S., Chatain, V., Hanna, K., 2014. Sorption of nalidixic acid onto micrometric and nanometric magnetites: experimental study and modeling. Appl. Surf. Sci. 299, 136–145.

Usman, M., Byrne, J.M., Chaudhary, A., Orsetti, S., Hanna, K., Ruby, C., Kappler, A., Haderlein, S.B., 2018. Magnetite and green rust: synthesis, properties, and environmental applications of mixed-valent iron minerals. Chem. Rev. 118, 3251–3304.

Wang, L., Li, J., Jiang, Q., Zhao, L., 2012. Water-soluble Fe_3O_4 nanoparticles with high solubility for removal of heavy-metal ions from waste water. Dalton Trans. 41, 4544–4551.

Weber, T.W., Chakravorti, R.K., 1974. Pore and solid diffusion models for fixed bed adsorbents. Am. Institute Chem. Eng. J. 20, 228–238.

Weijiang, Z., Yace, Z., Yuvaraja, G., Jiao, X., 2017. Adsorption of Pb(II) ions from aqueous environment using eco-friendly chitosan schiff`s base@Fe3O4 (CSB@ Fe3O4) as an adsorbent; kinetics, isotherm and thermodynamic studies. Int. J. Biol. Macromol. 105, 422–430.

Yean, S., Cong, L., Yavuz, C.T., Mayo, J.T., Yu, W.W., Kan, A.T., Colvin, V.L., Tomson, M. B., 2005. Effect of magnetite particle size on adsorption and desorption of arsenite and arsenate. J. Mater. Res. 20, 3255–3264.